Journal of the Optical Society of America B
OPTICAL PHYSICS

Two-dimensional atom localization via phase-sensitive absorption-gain spectra in five-level hyper inverted-Y atomic systems

Zhonghu Zhu,[1] Wen-Xing Yang,[1,2,*] Ai-Xi Chen,[3,4] Shaopeng Liu,[1] and Ray-Kuang Lee[2]

[1]Department of Physics, Southeast University, Nanjing 210096, China
[2]Institute of Photonics Technologies, National Tsing-Hua University, Hsinchu 300, Taiwan
[3]Institute for Quantum Computing, University of Waterloo, Waterloo, Ontario N2L 3G1, Canada
[4]Department of Applied Physics, East China Jiaotong University, Nanchang 330013, China
*Corresponding author: wenxingyang2@126.com

Received 26 February 2015; revised 5 April 2015; accepted 7 April 2015; posted 10 April 2015 (Doc. ID 235152); published 8 May 2015

A scheme for realizing two-dimensional atom localization in the sub-wavelength domain is proposed in a microwave-driven five-level hyper inverted-Y atomic system in which the atom interacts with a weak probe field, two control fields together with two orthogonal standing-wave fields. Because of the spatially dependent atom-field interaction, the information about the position of the atom can be extracted directly from the absorption and gain spectra of a weak probe field. It has been found that the probe detuning, the intensities of two control fields, and the relative phase of the driving fields can significantly improve the localization precision. Moreover, the maximal probability of finding the atom at an expected position in the sub-wavelength domain of the standing-wave field can reach unity via properly adjusting the system parameters.

OCIS codes: (020.1670) Coherent optical effects; (020.5580) Quantum electrodynamics.

http://dx.doi.org/10.1364/JOSAB.32.001070

1. INTRODUCTION

High-precision measurement of an atomic position through a standing-wave field has been the subject of active research over the past few decades because of its potential applications in laser cooling and trapping of neutral atoms [1,2], such as atom nanolithography [3,4], Bose-Einstein condensation [5–7], the measurement of the center-of-mass wave function of moving atoms [8,9], and coherent patterning of matter waves [10]. It is a well-known fact that many interesting optical phenomena have been proposed on the basis of atomic coherence and quantum interference such as four-wave mixing (FWM) [11–15], optical bistability (OB), optical multistability (OM) [16–18], electromagnetically induced transparency (EIT) [19–21], optical solitons [22], and giant Kerr nonlinearity [23–27]. More interestingly, a variety of schemes for realizing one-dimensional atom localization have been proposed on the basis of atomic coherence and quantum interference effects [28–37]. These schemes have demonstrated that the maximum probability of finding an atom at a particular position in a unit of wavelength of a standing-wave is 25%. Moreover, other techniques including EIT [38], dark resonances [39], spatially dependent spontaneous emission [40,41], probe absorption [42], and coherent population trapping (CPT) [43] can also be used to achieve one-dimensional atom localization. More recently, two-dimensional atom localization, achieved by applying two orthogonal standing-wave fields, has been studied extensively for its better prospect for application and its unique properties. For two-dimensional atom localization, Ivanov and Rozhdestvensky [44] presented a scheme for two-dimensional sub-wavelength localization in a four-level tripod system by measuring the population of the atom. Another related two-dimensional atom localization scheme was demonstrated in [45] by controlled spontaneous emission in a four-level atomic system with a closed loop. Since then, several high-precision and high-resolution two-dimensional atom localization schemes have been reported by Ding and coworkers [46,47] for a microwave-driven cycle-configuration atomic system and a microwave-driven four-level Y-type atomic system. The results of [46,47] have shown that the external microwave-driven field applied in a system plays an important role in improving the precision of two-dimensional atom localization. Inspired by these studies, we present a scheme for realizing high-precision two-dimensional atom localization in a microwave-driven five-level hyper inverted-Y atomic system.

In the present paper, we explore two-dimensional atom localization based on phase-sensitive probe absorption and gain in a microwave-driven five-level hyper inverted-Y atomic system. Since the microwave source is easier to obtain and manipulate

than an extra laser field, an application of particular interest is the microwave-driven field which is applied to drive the ground-state hyperfine transition. With the proper adjustment of the system parameters, a variety of localization patterns of an atom, such as lattice-like, crater-like and spike-like, can be observed under the joint actions of the standing-wave and microwave-driven fields. Additionally, there are three important results: (1) the atom can be localized at a particular position, and the maximum probability of finding an atom at a particular position within one period of standing-wave fields can reach 100% as long as the probe detuning is adjusted to an appropriate value; (2) the high-precision and high-resolution two-dimensional atom localization can be obtained via the application of two appropriate control fields; (3) the position of the localized atom is dependent on the relative phase of the driving fields, and a 100% probability of finding the atom at a particular position within one period of the standing-wave fields can be achieved only when the relative phase φ is equal to 0 or π. Furthermore, our scheme is based on the measurement of the probe absorption gain, which is much easier to carry out in the practical experiment than the measurement of spontaneous emission [45,46]. The reason is that spontaneous emission is a random process and the frequency of the spontaneously emitted photon is hard to control. At the same time, it is worth noting that our scheme may improve the localization precision and spatial resolution of the atom at an expected position by varying the system parameters. Therefore, our proposed scheme has more advantages than other schemes for two-dimensional atom localization.

2. THEORETICAL MODEL AND BASIC EQUATIONS

Let us consider a microwave-driven five-state atomic system in a hyper inverted-Y configuration as shown in Fig. 1(a). A weak probe field E_p (with angular frequency ω_p and a Rabi frequency $2\Omega_p$) couples the electric dipole transition between levels $|0\rangle$ and $|2\rangle$ (with transition frequency ω_{20}). An extra microwave-driven field (with a Larmor frequency $2\Omega_{mw}$) is used to resonantly couple the two hyperfine levels $|0\rangle$ and $|1\rangle$ through an allowed magnetic dipole transition. The two control fields, E_c (with angular frequency ω_c and a Rabi frequency $2\Omega_c$) and E_d (with angular frequency ω_d and a Rabi frequency $2\Omega_d$), drive the electric dipole transitions between levels $|2\rangle$ and $|3\rangle$ (with transition frequency ω_{32}) and between levels $|3\rangle$ and $|4\rangle$ (with transition frequency ω_{43}), respectively. The transition between levels $|1\rangle$ and $|2\rangle$ (with transition frequency ω_{21}) is coupled by the composition of two orthogonal standing-wave fields with position-dependent Rabi frequency $2G_s(x,y) = 2\Omega_s[\sin(\kappa x) + \sin(\kappa y)]$, where $\kappa = \omega_s/c$ is the same wave vector of the two laser fields. The probe field Ω_p, as well as two control fields, $\Omega_{c,d}$ and microwave Ω_{mw}, propagate along the z direction, and an atom moves along the z direction and passes through the intersectant region of the two orthogonal standing-wave fields in the x–y plane. As a result, the interaction between the atom and the standing-wave fields is spatial dependent on the x–y plane. Inspecting the system, we find that states $|0\rangle$, $|2\rangle$, $|3\rangle$, and $|4\rangle$ are in a four-state cascade-type system, while the transitions $|0\rangle \overset{\Omega_{mw}}{\longleftrightarrow} |1\rangle \overset{G_s(x,y)}{\longleftrightarrow} |2\rangle \overset{\Omega_p}{\longleftrightarrow} |0\rangle$ form a typical

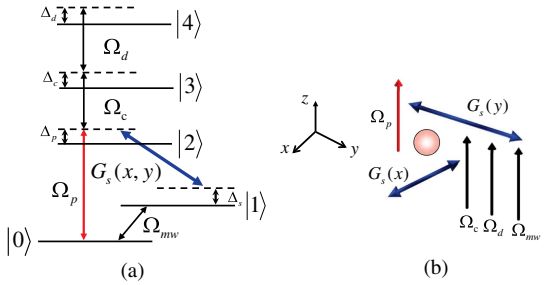

Fig. 1. (a) Energy-level diagram of a microwave-driven five-level hyper inverted-Y atomic system interacting with a weak probe field Ω_p, two control fields $\Omega_{c,d}$ and a combination of two orthogonal standing waves $G_s(x,y)$, where $G_s(x,y)$ is a combination of two orthogonal standing waves, and Ω_{mw} is the half Larmor frequency for the respective driven transition. Δ_p represents the single-photon detuning, Δ_s and Δ_c are two separate two-photon detunings, respectively, and Δ_d stands for the three-photon detuning. (b) Two standing-wave fields, $G_s(x)$ and $G_s(y)$, propagating in perpendicular directions form the intersectant region in the x–y plane, while the probe field Ω_p, as well as two control fields, $\Omega_{c,d}$ and microwave Ω_{mw}, propagate along the z direction.

three-state Λ-type cyclic configuration. Hence, the five-level hyper inverted-Y system [shown in Fig. 1(a)] consists of two subsystems.

Here we assume that the center-of-mass position distribution of the atom along the directions of the standing-wave fields is nearly constant and we can ignore the kinetic energy of the atom in the Hamiltonian via applying the Raman–Nath approximation [48]. By choosing $H_0 = (\omega_p - \omega_s)|1\rangle\langle 1| + \omega_p|2\rangle\langle 2| + (\omega_p + \omega_c)|3\rangle\langle 3| + (\omega_p + \omega_c + \omega_d)|4\rangle\langle 4|$ and taking level $|0\rangle$ as the energy origin, under the electric dipole approximation (EDA) and the rotating-wave approximation (RWA), the interaction Hamiltonian of the present atomic system is given by ($\hbar = 1$)

$$\begin{aligned} H_I = &-\Delta_s|1\rangle\langle 1| - \Delta_p|2\rangle\langle 2| - \Delta_c|3\rangle\langle 3| - \Delta_d|4\rangle\langle 4| \\ &- [\Omega_p|2\rangle\langle 0| + \Omega_c|3\rangle\langle 2| \\ &+ \Omega_d|4\rangle\langle 3| + G_s(x,y)|2\rangle\langle 1| + \Omega_{mw}|1\rangle\langle 0| + \text{H.c.}], \end{aligned} \quad \textbf{(1)}$$

where the symbol H.c. represents the Hermitian conjugation. $\Delta_p = \omega_p - \omega_{20}$ represents the single-photon detuning, $\Delta_s = \omega_p - \omega_s - \omega_{10}$ and $\Delta_c = \omega_p + \omega_c - \omega_{30}$ are two separate two-photon detunings, respectively, and $\Delta_d = \omega_p + \omega_c + \omega_d - \omega_{40}$ stands for the three-photon detuning. $\Omega_p = \mu_{20}E_p/(2\hbar)$, $\Omega_c = \mu_{32}E_c/(2\hbar)$, $\Omega_d = \mu_{43}E_d/(2\hbar)$, and $G_s(x,y) = \Omega_s[\sin(\kappa x) + \sin(\kappa y)]$ with $\Omega_s = \mu_{21}E_s/(2\hbar)$ are the half Rabi frequencies of the laser fields for the relevant driven transitions. It is worth noting that $\Omega_{mw} = \mu_{10}B_{mw}/(2\hbar)$ is the half Larmor frequency for the respective driven transition, where B_{mw} is the amplitude of the microwave-driven field and $\mu_{ij} = \vec{\mu}_{ij} \cdot \vec{e}_L$ $(i,j = 0\text{–}4)$ denotes the dipole matrix moment for the relevant optical transition from level $|i\rangle$ to level $|j\rangle$ with $\vec{e}_L$ denoting the unit polarization vector of the corresponding laser field. In the following calculations, we set Ω_c and Ω_d as real parameters, while Ω_p, Ω_s, and Ω_{mw} are set as complex parameters, i.e., $\Omega_p = |\Omega_p|e^{i\varphi_p}$, $\Omega_s = |\Omega_s|e^{i\varphi_s}$, and $\Omega_{mw} = |\Omega_{mw}|e^{i\varphi_m}$, where φ_p, φ_s and φ_m are the phases of the weak probe field, the

combination of two orthogonal standing-wave fields and the microwave-driven field, respectively.

The dynamics of this system can be described by using the probability amplitude equations. Then the wave function of the present atomic system at time t can be expressed in terms of the state vectors as

$$|\psi(t)\rangle = \iint \mathrm{d}x\mathrm{d}y f(x,y)|x\rangle|y\rangle[A_0(x,y;t)|0\rangle + A_1(x,y;t)|1\rangle + A_2(x,y;t)|2\rangle + A_3(x,y;t)|3\rangle + A_4(x,y;t)|4\rangle], \quad (2)$$

where $A_i(x,y;t)$ $(i = 0\text{–}4)$ denotes the time- and position-dependent probability amplitude for the atom in level $|i\rangle$, and $f(x,y)$ is the center-of-mass wave function of the atom.

Hence, the conditional position probability distribution, i.e., the probability of finding the atom in the (x,y) position at time t in the standing-wave fields when the atom is found in its internal state $|2\rangle$, can be given by

$$P(x,y;t|2) = |\mathcal{N}|^2|f(x,y)|^2|A_2(x,y;t)|^2, \quad (3)$$

where $\mathcal{N}$ is a normalization factor. Here, we assume that the center-of-mass wave function of the atom $f(x,y)$ is nearly constant over many wavelengths of the standing-wave fields in the x–y plane, which remains unchanged, even after the interaction with the optical fields. That is to say, the conditional position probability distribution $P(x,y;t|2)$ is mainly determined by the term $|A_2(x,y;t)|^2$. Therefore, the measurement of the population in level $|2\rangle$ can directly obtain the position information of the atom when the atom passes through the standing-wave fields.

By substituting the interaction Hamiltonian given by Eq. (1) and the atomic wave function given by Eq. (2) into the time-dependent Schrödinger wave equation $i\partial|\psi(t)\rangle/\partial t = H_I|\psi(t)\rangle$, the coupled equations of motion for the time evolution of the atomic probability amplitudes can be given as

$$\frac{\partial A_0(t)}{\partial t} = i\Omega_{mw}^* A_1(t) + i\Omega_p^* A_2(t), \quad (4)$$

$$\frac{\partial A_1(t)}{\partial t} = i(\Delta_s + i\gamma_1)A_1(t) + iG_s^*(x,y)A_2(t) + i\Omega_{mw}A_0(t), \quad (5)$$

$$\frac{\partial A_2(t)}{\partial t} = i(\Delta_p + i\gamma_2)A_2(t) + iG_s(x,y)A_1(t) + i\Omega_c^* A_3(t) + i\Omega_p A_0(t), \quad (6)$$

$$\frac{\partial A_3(t)}{\partial t} = i(\Delta_c + i\gamma_3)A_3(t) + i\Omega_d^* A_4(t) + i\Omega_c A_2(t), \quad (7)$$

$$\frac{\partial A_4(t)}{\partial t} = i(\Delta_d + i\gamma_4)A_4(t) + i\Omega_d A_3(t), \quad (8)$$

where γ_i are the decay rates of states $|i\rangle$ $(i = 1\text{–}4)$ which are added phenomenologically.

Under the weak-field approximation, i.e., $\Omega_p \ll \Omega_c, \Omega_d$, we can get $A_0(x,y;t) \approx 1$ for all of the time t in the condition of considering the quasi-stationary-state solution of Eqs. (5)–(8). Then, the probability amplitude $A_2(x,y;t)$ in the large time limit can be derived as

$$A_2(x,y) = \frac{(|G_s(x,y)||\Omega_{mw}|e^{i(\varphi_s+\varphi_m)} - a|\Omega_p|e^{i\varphi_p})(cd - |\Omega_d|^2)}{abcd - cd|G_s(x,y)|^2 - ad|\Omega_c|^2 - ab|\Omega_d|^2 + |G_s(x,y)|^2|\Omega_d|^2}, \quad (9)$$

where $a = \Delta_s + i\gamma_1$, $b = \Delta_p + i\gamma_2$, $c = \Delta_c + i\gamma_3$ and $d = \Delta_d + i\gamma_4$.

On the other hand, we can also obtain the absorption of the weak probe field from the imaginary part of the susceptibility given as

$$\chi_p''(x,y) = \mathrm{Im}[\chi_p(x,y)] = \frac{N|\mu_{20}|^2}{2\hbar\varepsilon_0}|f(x,y)|^2\mathrm{Im}[\tilde{\chi}_p(x,y)], \quad (10)$$

where the parameters N and ε_0 present the atomic number density and the vacuum dielectric constant, respectively, and

$$\tilde{\chi}_p(x,y) = \frac{A_2(x,y)A_0^*(x,y)}{\Omega_p} = \frac{\left(\frac{|G_s(x,y)||\Omega_{mw}|}{|\Omega_p|}e^{i\varphi} - a\right)\left(cd - |\Omega_d|^2\right)}{abcd - cd|G_s(x,y)|^2 - ad|\Omega_c|^2 - ab|\Omega_d|^2 + |G_s(x,y)|^2|\Omega_d|^2}, \quad (11)$$

where $\varphi = \varphi_s + \varphi_m - \varphi_p$ denotes the relative phase of three driving fields. The relative phase φ can effectively affect the behavior of two-dimensional atom localization, which can also be verified by the following section.

Giving insight into Eqs. (3) and (9)–(11), we find that they are in direct proportion to the same factor, which presents that the measurement of the probe field absorption spectra can also directly provide the position information of the atom when the atom passes through the standing-wave fields. In another words, the peak position of the probe absorption denotes where the atom is localized, and the peak number of the probe absorption in one period of the standing-wave fields means the conditional position probability of finding the atom at a particular position. For convenience, we define the filter function given as

$$F(x,y) = \mathrm{Im}[\tilde{\chi}_p(x,y)]. \quad (12)$$

Therefore, measuring the probe absorption spectra under proper conditions can localize the atom at a particular position within one period of standing-wave fields in the x–y plane.

3. NUMERICAL RESULTS AND DISCUSSION

We now discuss the conditional position probability distribution of the atom via a few numerical calculations based on the filter function in Eq. (12), and then achieve high-precision two-dimensional atom localization via measuring the probe absorption and gain spectra. Here, a realistic candidate for the proposed atomic system can be found in ^{87}Rb atoms with the designated states chosen as follows [21,49]: $|5S_{1/2}, F = 1, m_F = 0\rangle$ as $|0\rangle$, $|5S_{1/2}, F = 2, m_F = 0\rangle$ as $|1\rangle$, $|5P_{1/2}\rangle$ as $|2\rangle$, $|5D_{3/2}\rangle$ as $|3\rangle$, and $|nP_{3/2}\rangle (n > 10)$ as $|4\rangle$. The respective transitions are $|0\rangle \leftrightarrow |2\rangle$ at 795 nm, $|2\rangle \leftrightarrow |3\rangle$ at 762 nm, and $|3\rangle \leftrightarrow |4\rangle$ at 1.3–1.5 μm [20]. Thus, the decay rates of excited states $|1\rangle$, $|2\rangle$, $|3\rangle$, and $|4\rangle$ are $\Gamma_1 = 2\gamma_1 \simeq 11.2$ kHz, $\Gamma_2 = 2\gamma_2 \simeq 11.2$ MHz, $\Gamma_3 = 2\gamma_3 \simeq 1.52$ MHz and $\Gamma_4 = 2\gamma_4 \simeq 0.16$ MHz, respectively. To give a clear illustration, we select $\Delta_c = \Delta_d \simeq 3.92$ MHz $= 0.7\gamma_2$, and all the parameters used in the following numerical calculations are in the unit of γ_2. Subsequently, as shown in Figs. 2–5, we obtain a few numerical results for two-dimensional atom localization with different values of the relevant parameters to illustrate that the high-precision two-dimensional atom localization can be achieved in the present five-level hyper inverted-Y-type atomic system.

In the absence of the relative phase φ (i.e., $\varphi = 0$), we analyze how the frequency detuning of the weak probe field Δ_p modify the behavior of two-dimensional atom localization. In Fig. 2, we show the filter function $F(x, y)$ versus the normalized positions $(\kappa x, \kappa y)$ in dependence on the detuning Δ_p of the probe field. The corresponding density plots are illustrated in Fig. 3. From Figs. 2(a) and 3(a), when the probe field is in resonance with the corresponding transition (i.e., $\Delta_p = 0$), it's shown that the peak maxima of the probe absorption are distributed on the diagonal in the second and fourth quadrants of the x–y plane with a lattice-like pattern, where the atom localization peaks are determined by $\kappa x + \kappa y = 2n\pi$ or $\kappa x - \kappa y = (2m + 1)\pi$ (n, m are integers). As the probe detuning Δ_p increases with all other parameters keeping fixed, the peak maxima of the filter function $F(x, y)$ are situated in the four quadrants but with different probability, and are mainly localized in the third quadrant with a crater-like pattern, which shows that the spatial resolution of atomic position is very poor as shown in Figs. 2(b) and 3(b). Interestingly, when the probe detuning is tuned to $\Delta_p = 14\gamma_2$, the filter function exhibits a crater-like pattern in the first and third quadrants with different localization precision as shown in Figs. 2(c) and 3(c), where localization peaks in the third quadrant have a higher precision and resolution than that shown in the first quadrant. Furthermore, with the further increase of the probe detuning Δ_p (i.e., $\Delta_p = 20\gamma_2$), it can be seen from Figs. 2(d) and 3(d) that the atom is completely localized in the third quadrant with the very sharp localization peak. In this case, the atom is localized at the position $(\kappa x, \kappa y) = (-\pi/2, -\pi/2)$ with a 100% probability of finding the atom at an expected spatial position within one period of the standing-wave fields. Thus, the high-precision and high-resolution of two-dimensional atom localization is indeed achieved via adjusting the probe detuning. What's more, the spatial resolution of atomic position is greatly improved compared to Figs. 2(a)–2(c).

In Fig. 4, we investigate the influences of intensities of two control fields, Ω_c and Ω_d, on the filter function $F(x, y)$ without

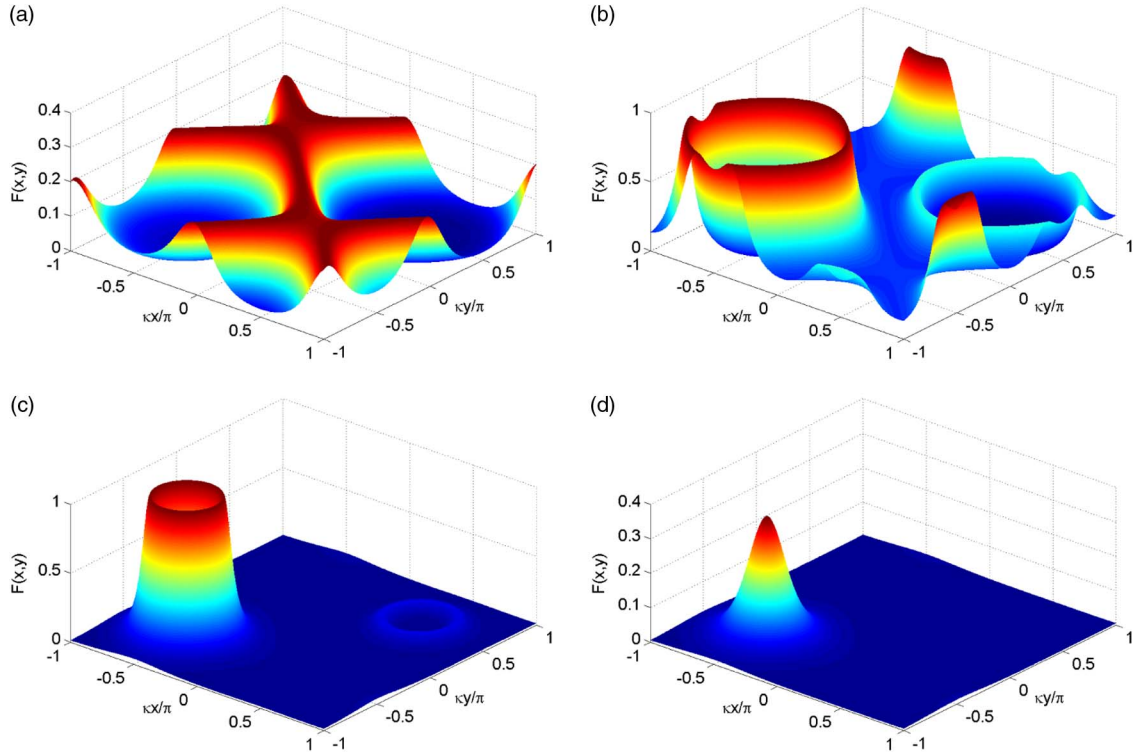

Fig. 2. Filter function $F(x, y)$ as a function of $(\kappa x, \kappa y)$ with different frequency detuning Δ_p of the probe field. (a) $\Delta_p = 0$, (b) $\Delta_p = 5.5\gamma_2$. (c) $\Delta_p = 14\gamma_2$, and (d) $\Delta_p = 20\gamma_2$. Other values of the parameters were chosen as $\gamma_1 = 0.001\gamma_2$, $\gamma_2 \simeq 5.6$ MHz, $\gamma_3 = 0.1357\gamma_2$, $\gamma_4 = 0.0143\gamma_2$, $\Delta_s = 0.17\gamma_2$, $\Delta_c = \Delta_d = 0.7\gamma_2$, $\Omega_c = 1.1\gamma_2$, $\Omega_d = 0.4\gamma_2$, $\Omega_s = 0.8\gamma_2$, $|\Omega_{mw}| = 0.001\gamma_2$, $\Omega_p = 0.01\gamma_2$, and $\varphi = 0$.

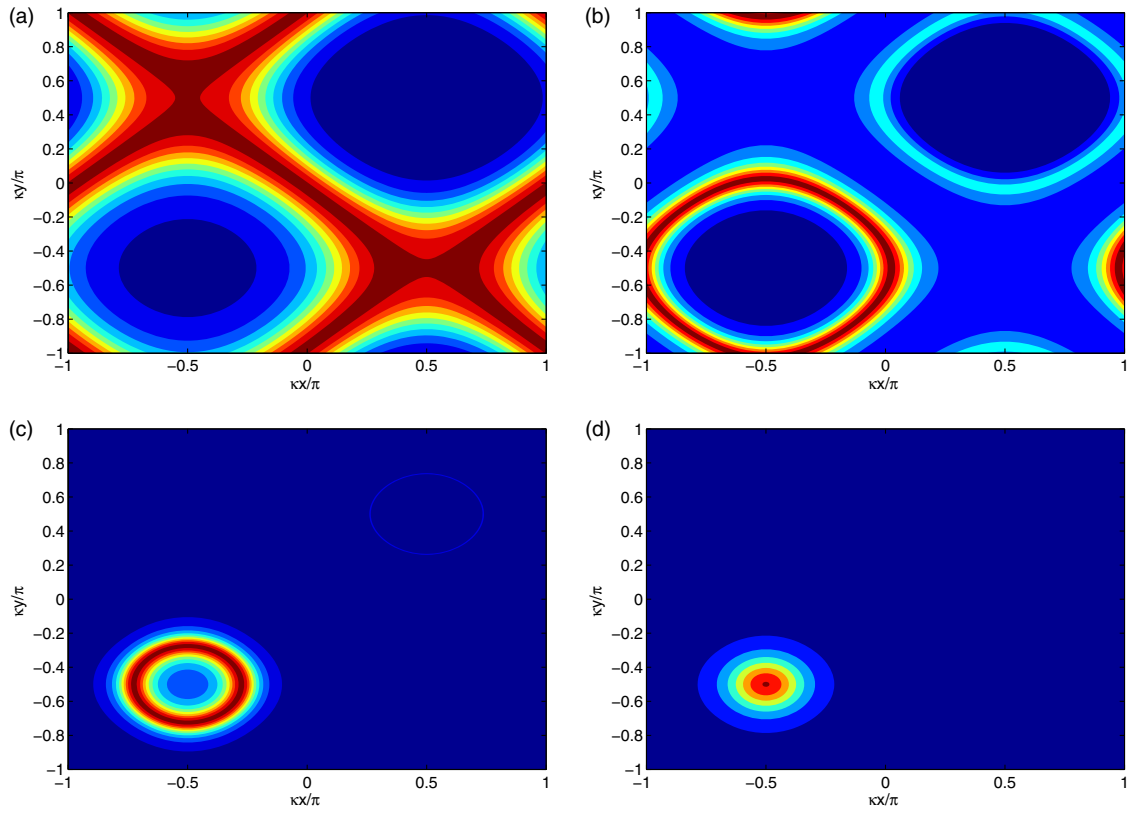

Fig. 3. Density plot of filter function in the plane shown in Fig. 2.

considering the relative phase φ (i.e., $\varphi = 0$). From Fig. 4, we present that the spatial distribution and the probability of finding the atom at a particular position in one period of the standing-wave fields is dependent on the two control fields. In the case of $(\Omega_c, \Omega_d) = (1.1\gamma_2, 0.3\gamma_2)$, the absorption peaks are mostly distributed in the third quadrant of the x–y plane with a crater-like pattern and, with little in the first quadrant, in which the atom is localized at the circular edges of the two craters. When the intensity of the control field Ω_d increases to $0.8\gamma_2$ with keeping Ω_c fixed as shown in Fig. 4(b), the probe-absorption maxima are only situated in the third quadrant at the expected position $(\kappa x, \kappa y) = (-\pi/2, -\pi/2)$ with a spike-like pattern, and the maximal probability of finding the atom at an expected position in the sub-wavelength domain of the standing-wave field is increased to unity. However, it can be seen from Fig. 4(c) that with increasing Ω_d from $0.8\gamma_2$ to $0.98\gamma_2$, the crater-like localization peaks appear again in the first and third quadrants when all other parameters are kept fixed, where the localization precision of the third quadrant is much higher than that shown in the first quadrant. For further investigation of how the intensity of another control field Ω_c affects the behavior of two-dimensional atom localization, we plot the filter function $F(x, y)$ versus the normalized position $(\kappa x, \kappa y)$ for different intensities of the control field Ω_c as shown in Figs. 4(d)–4(e). In the case that $(\Omega_c, \Omega_d) = (0.8\gamma_2, 0.9\gamma_2)$, the result is similar to the result of Fig. 4(c), and the atom is localized at the circular edges of the craters with a low-precision crater-like pattern in the first quadrant and another high-precision crater-like pattern in the third quadrant. More interestingly, when there is an increase in the intensity of the control field Ω_c, i.e., $(\Omega_c, \Omega_d) = (1.5\gamma_2, 0.9\gamma_2)$, the peak maxima of the absorption spectrum are completely localized at position $(\kappa x, \kappa y) = (-\pi/2, -\pi/2)$ in the third quadrant with a sharp spike-like pattern, as illustrated in Fig. 4(e), which is similar to Fig. 4(b). In such a case, the detecting probability of the atom at an expected position in one period of the standing-wave fields is 100%. From the above discussions, it is demonstrated that the application of two appropriate control fields, such as $(\Omega_c, \Omega_d) = (1.1\gamma_2, 0.8\gamma_2)$ and $(\Omega_c, \Omega_d) = (1.5\gamma_2, 0.9\gamma_2)$, leads to a 100% probability of finding the atom at an expected position in one period of the standing-wave fields. As a result, the high-precision and high-resolution two-dimensional atom localization can be obtained via modulating the appropriate intensities of the two control fields.

As a matter of fact, we are particularly interested in the influence of the relative phase φ on the behavior of two-dimensional atom localization, which is one of the most interesting characteristics of the present atomic system. In Fig. 5, we present numerical results for the analysis of the relative phase φ on the filter function $F(x, y)$ as a function of $(\kappa x, \kappa y)$. Because the values of the system parameters in Fig. 5(a) are the same as in Fig. 2(d), we can obtain the same results as Fig. 2(d). Then, when $\varphi = \pi/3$, another high-precision localization peak with a spike-like pattern appears in the first quadrant, and the localization peak in the third quadrant is greatly suppressed and becomes smaller as shown in Fig. 5(b). As the relative phase is tuned to $\varphi = 2\pi/3$ in Fig. 5(c), the peak maxima of the probe gain-absorption spectra are still localized at a certain position with

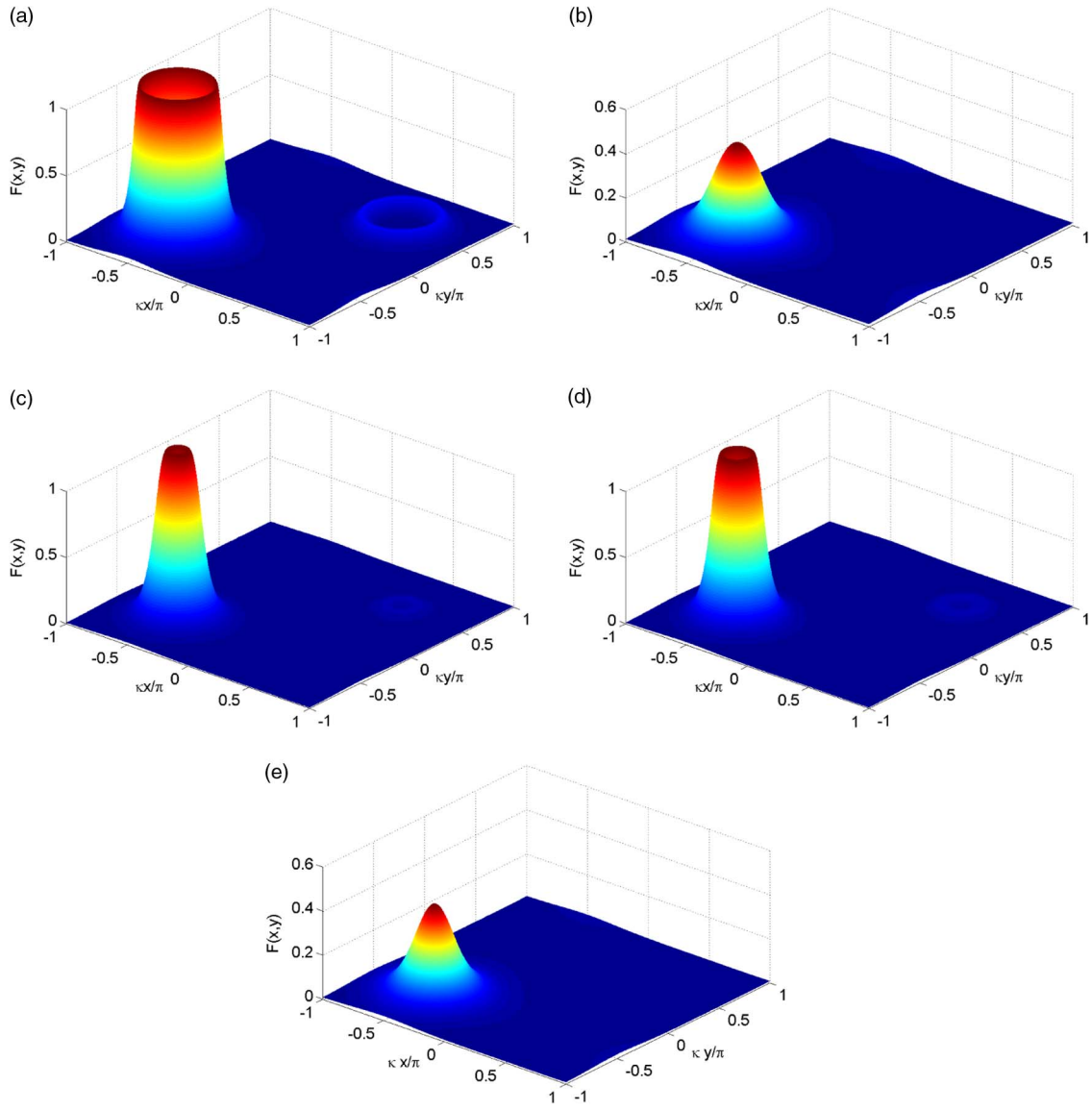

Fig. 4. Filter function $F(x, y)$ as a function of $(\kappa x, \kappa y)$ with different intensities of two control fields, Ω_c and Ω_d. (a) $(\Omega_c, \Omega_d) = (1.1\gamma_2, 0.3\gamma_2)$, (b) $(\Omega_c, \Omega_d) = (1.1\gamma_2, 0.8\gamma_2)$, (c) $(\Omega_c, \Omega_d) = (1.1\gamma_2, 0.98\gamma_2)$, (d) $(\Omega_c, \Omega_d) = (0.8\gamma_2, 0.9\gamma_2)$, and (e) $(\Omega_c, \Omega_d) = (1.5\gamma_2, 0.9\gamma_2)$. Other values of the parameters are the same as in Fig. 2, except for $\Delta_p = 13\gamma_2$.

a spike-like pattern in the first quadrant and inverted-spike-like pattern in the third quadrant. For this case, it is worth pointing out that $F(x, y) > 0$ corresponds to absorption of the probe field, whereas $F(x, y) < 0$ corresponding to the probe field is amplified by the atom. In other words, it is sure that the atom is passing through the standing-wave fields around the position $(\kappa x, \kappa y) = (\pi/2, \pi/2)$ in the first quadrant; however, the atom must locate at the position $(\kappa x, \kappa y) = (-\pi/2, -\pi/2)$ in the third quadrant. Furthermore, for the case $\varphi = \pi$, the probe-absorption maxima is completely situated in the first quadrant at the position $(\kappa x, \kappa y) = (\pi/2, \pi/2)$ with a spike-like pattern, which is the mirror reflection of the localization pattern observed in Fig. 5(a). In a word, the behavior of two-dimensional atom localization is sensitive to the relative phase φ, and we can obtain a 100% probability of finding the atom at a particular position within one period of the standing-wave fields via tuning the relative phase to $\varphi = 0$ or $\varphi = \pi$. Finally, it is worth noting that such high-precision and high-resolution two-dimensional atom localization originates from the destructive quantum interference induced by the microwave-driven field because of the existence of two possible pathways from state $|0\rangle$ to state $|2\rangle$: the direct one $|0\rangle \overleftrightarrow{\Omega_p} |2\rangle$ and the indirect one $|0\rangle \overleftrightarrow{\Omega_{mw}} |1\rangle \overleftrightarrow{G_s(x, y)} |2\rangle$.

4. CONCLUSIONS

In conclusion, we have analyzed in detail the behaviors of two-dimensional atom localization in a five-level hyper inverted-Y atomic system based on the measurements of the probe absorption and gain spectra, in which the hyperfine

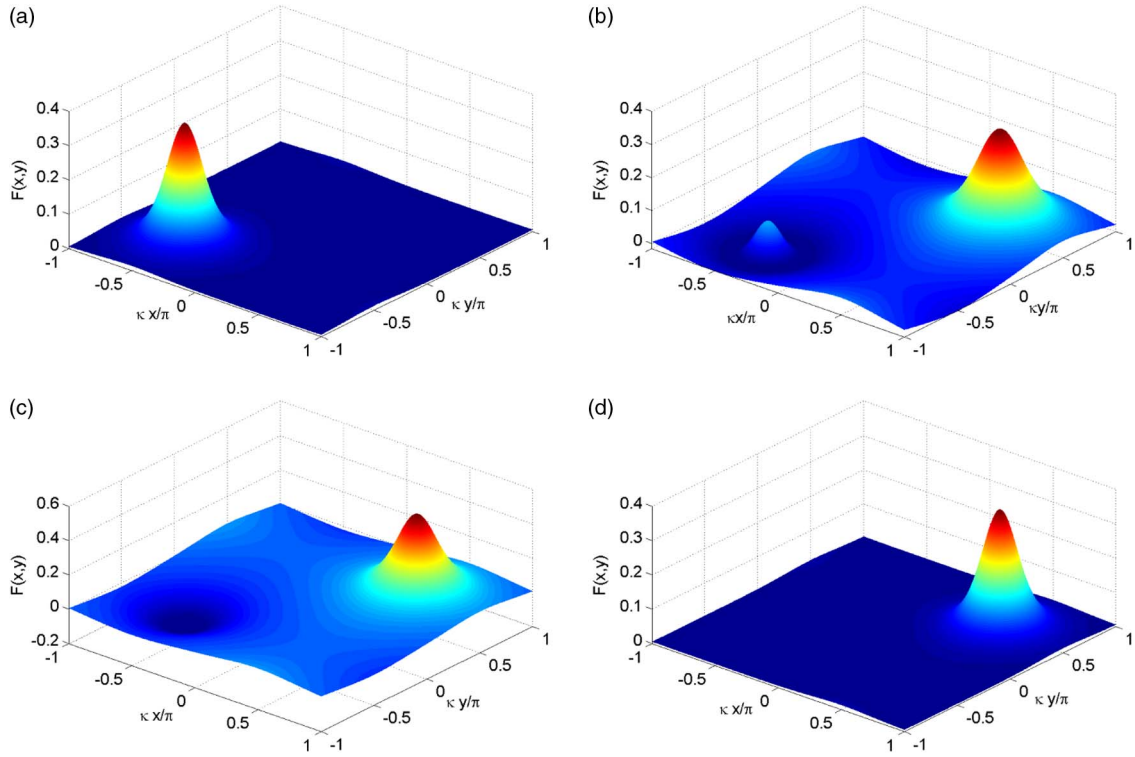

Fig. 5. Filter function $F(x, y)$ as a function of $(\kappa x, \kappa y)$ in dependence on the relative phase φ. (a) $\varphi = 0$, (b) $\varphi = \pi/3$, (c) $\varphi = 2\pi/3$, and (d) $\varphi = \pi$. Other values of the parameters are the same as in Fig. 2, except for $\Omega_c = 1.1\gamma_2$, $\Omega_d = 0.4\gamma_2$, and $\Delta_p = 20\gamma_2$.

transition between the two ground levels is resonantly coupled by an extra microwave-driven field. Because of the spatial-position-dependent atom-field interaction, two-dimensional atom localization can be achieved by the measurements of the probe absorption and gain spectra. It was clearly shown that the precision of two-dimensional atom localization is extremely sensitive to the detuning of the weak probe field, the intensities of the two control fields, and the relative phase of the driving fields. The main advantage of our proposed scheme is that the maximum probability of finding the atom at an expected position in one period of the standing-wave fields is 100%, which originated from the joint quantum interference induced by the combination of two orthogonal standing-wave fields, the two control fields, and the microwave-driven field. Finally, it is worth noting that our absorption-measurement scheme provides a possibility to observe two-dimensional atom localization in the experiment, because the absorption measurement is much easier to carry out in a laboratory compared to the measurement of spontaneous emission.

Before ending, we should note that the present study focuses only on the cold atomic system; the results of Doppler broadening effects can be included by first rewriting the corresponding detunings, i.e., $\Delta_p = \omega_p - \omega_{20} - \Delta_{a1}$, $\Delta_s = \omega_p - \omega_s - \omega_{10} - \Delta_{a2}$, $\Delta_c = \omega_p + \omega_c - \omega_{30} - \Delta_{a3}$, and $\Delta_d = \omega_p + \omega_c + \omega_d - \omega_{40} - \Delta_{a4}$ with $\Delta_{a1} \sim k_p$, $\Delta_{a2} \sim k_p - k_s$, $\Delta_{a3} \sim k_p + k_c$, and $\Delta_{a2} \sim k_p + k_c + k_d$ the corresponding additional broadening effects, which can be suppressed in the cold atomic system.

National Natural Science Foundation of China (NSFC) (11374050, 61372102).

We would like to thank Professor Ying Wu for his encouragement and helpful discussion.

REFERENCES

1. H. Metcalf and P. Van der Straten, "Cooling and trapping of neutral atoms," Phys. Rep. **244**, 203–286 (1994).
2. W. D. Phillips, "Nobel lecture: Laser cooling and trapping of neutral atoms," Rev. Mod. Phys. **70**, 721–741 (1998).
3. K. S. Johnson, J. H. Thywissen, W. H. Dekker, K. K. Berggren, A. P. Chu, R. Younkin, and M. Prentiss, "Localization of metastable atom beams with optical standing waves: nanolithography at the Heisenberg limit," Science **280**, 1583–1586 (1998).
4. A. N. Boto, P. Kok, D. S. Abrams, S. L. Braunstein, C. P. Williams, and J. P. Dowling, "Quantum interferometric optical lithography: exploiting entanglement to beat the diffraction limit," Phys. Rev. Lett. **85**, 2733–2736 (2000).
5. G. P. Collins, "Experimenters produce new Bose-Einstein condensate(s) and possible puzzles for theorists," Phys. Today **49**(3), 18–21 (1996).
6. Y. Wu, X. X. Yang, and C. P. Sun, "Systematic method to study the general structure of Bose-Einstein condensates with arbitrary spin," Phys. Rev. A **62**, 063603 (2000).
7. Y. Wu and R. Côté, "Bistability and quantum fluctuations in coherent photoassociation of a Bose-Einstein condensate," Phys. Rev. A **65**, 053603 (2002).
8. K. T. Kapale, S. Qamar, and M. S. Zubairy, "Spectroscopic measurement of an atomic wave function," Phys. Rev. A **67**, 023805 (2003).
9. J. Evers, S. Qamar, and M. S. Zubairy, "Atom localization and center-of-mass wave-function determination via multiple simultaneous quadrature measurements," Phys. Rev. A **75**, 053809 (2007).
10. J. Mompart, V. Ahufinger, and G. Birkl, "Coherent pattern of matter waves with subwavelength localization," Phys. Rev. A **79**, 053638 (2009).

11. Y. Wu and X. Yang, "Highly efficient four-wave mixing in double-Λ system in ultraslow propagation regime," Phys. Rev. A **70**, 053818 (2004).
12. S. P. Liu, W. X. Yang, Y. L. Chuang, A. X. Chen, A. Liu, Y. Huang, and R.-K. Lee, "Enhanced four-wave mixing efficiency in four-subband semiconductor quantum wells via Fano-type interference," Opt. Express **22**, 29179–29190 (2014).
13. Y. P. Zhang, U. Khadka, B. Anderson, and M. Xiao, "Controlling four-wave and six-wave mixing processes in multilevel atomic systems," Appl. Phys. Lett. **91**, 221108 (2007).
14. Y. P. Zhang, B. Anderson, A. W. Brown, and M. Xiao, "Competition between two four-wave mixing channels via atomic coherence," Appl. Phys. Lett. **91**, 061113 (2007).
15. Y. P. Zhang, A. W. Brown, and M. Xiao, "Opening four-wave mixing and six-wave mixing channels via dual electromagnetically induced transparency windows," Phys. Rev. Lett. **99**, 123603 (2007).
16. A. Joshi and M. Xiao, "Optical multistability in three-level atoms inside an optical ring cavity," Phys. Rev. Lett. **91**, 143904 (2003).
17. Z. Wang, A. X. Chen, Y. Bai, W. X. Yang, and R. K. Lee, "Coherent control of optical bistability in an open Λ-type three-level atomic system," J. Opt. Soc. Am. B **29**, 2891–2896 (2012).
18. Z. H. Zhu, A. X. Chen, W. X. Yang, and R.-K. Lee, "Phase knob for switching steady-state behaviors from bistability to multistability via spontaneously generated coherence," J. Opt. Soc. Am. B **31**, 2061–2067 (2014).
19. M. Fleischhauer, A. Imamoglu, and J. P. Marangos, "Electromagnetically induced transparency: optics in coherent media," Rev. Mod. Phys. **77**, 633–673 (2005).
20. Y. Wu, J. Saldana, and Y. F. Zhu, "Large enhancement of four-wave mixing by suppression of photon absorption from electromagnetically induced transparency," Phys. Rev. A **67**, 013811 (2003).
21. Y. Wu, L. L. Wen, and Y. F. Zhu, "Efficient hyper-Raman scattering in resonant coherent media," Opt. Lett. **28**, 631–633 (2003).
22. W. X. Yang, A. X. Chen, L. G. Si, K. Jiang, X. Yang, and R. K. Lee, "Three-coupled ultraslow temporal solitons in a five-level tripod atomic system," Phys. Rev. A **81**, 023814 (2010).
23. Y. P. Niu, S. Q. Gong, R. X. Li, Z. Z. Xu, and X. Y. Liang, "Giant Kerr nonlinearity induced by interacting dark resonances," Opt. Lett. **30**, 3371–3373 (2005).
24. D. D. Yavuz and D. E. Sikes, "Giant Kerr nonlinearities using refractive-index enhancement," Phys. Rev. A **81**, 035804 (2010).
25. Y. Wu and X. Yang, "Giant Kerr nonlinearities and solitons in a crystal of molecular magnets," Appl. Phys. Lett. **91**, 094104 (2007).
26. F. Dell'Anno, S. De Siena, and F. Illuminati, "Multiphoton quantum optics and quantum state engineering," Phys. Rep. **428**, 53–168 (2006).
27. A. Serafini, F. Illuminati, M. G. A. Paris, and S. De Siena, "Entanglement and purity of two-mode Gaussian states in noisy channels," Phys. Rev. A **69**, 022318 (2004).
28. E. Paspalakis and P. L. Knight, "Localizing an atom via quantum interference," Phys. Rev. A **63**, 065802 (2001).
29. S. Qamar, S. Y. Zhu, and M. S. Zubairy, "Atom localization via resonance fluorescence," Phys. Rev. A **61**, 063806 (2000).
30. P. Storey, M. Collett, and D. Walls, "Measurement-induced diffraction and interference of atoms," Phys. Rev. Lett. **68**, 472–475 (1992).
31. P. Storey, M. Collett, and D. Walls, "Atomic-position resolution by quadrature-field measurement," Phys. Rev. A **47**, 405–418 (1993).
32. R. Quadt, M. Collett, and D. F. Walls, "Measurement of atomic motion in a standing light field by homodyne detection," Phys. Rev. Lett. **74**, 351–354 (1995).
33. F. L. Kien, G. Rempe, W. P. Schleich, and M. S. Zubairy, "Atom localization via Ramsey interferometry: a coherent cavity field provides a better resolution," Phys. Rev. A **56**, 2972–2977 (1997).
34. M. Macovei, J. Evers, C. H. Keitel, and M. S. Zubairy, "Localization of atomic ensembles via superfluorescence," Phys. Rev. A **75**, 033801 (2007).
35. K. T. Kapale and M. S. Zubairy, "Subwavelength atom localization via amplitude and phase control of the absorption spectrum. II," Phys. Rev. A **73**, 023813 (2006).
36. H. Nha, J. H. Lee, J. S. Chang, and K. An, "Atomic-position localization via dual measurement," Phys. Rev. A **65**, 033827 (2002).
37. Z. P. Wang, B. L. Yu, J. Zhu, Z. G. Cao, S. L. Zhen, X. Q. Wu, and F. Xu, "Atom localization via controlled spontaneous emission in a five-level atomic system," Ann. Phys. **327**, 1132–1145 (2012).
38. N. A. Proite, Z. J. Simmons, and D. D. Yavuz, "Observation of atomic localization using electromagnetically induced transparency," Phys. Rev. A **83**, 041803(R) (2011).
39. C. P. Liu, S. Q. Gong, D. C. Cheng, X. J. Fan, and Z. Z. Xu, "Atom localization via interference of dark resonances," Phys. Rev. A **73**, 025801 (2006).
40. F. Ghafoor, S. Qamar, and M. S. Zubairy, "Atom localization via phase and amplitude control of the driving field," Phys. Rev. A **65**, 043819 (2002).
41. J. Xu and X. M. Hu, "Sub-half-wavelength atom localization via bichromatic phase control of spontaneous emission," Phys. Lett. A **366**, 276–281 (2007).
42. M. Sahrai, H. Tajalli, K. T. Kapale, and M. S. Zubairy, "Subwavelength atom localization via amplitude and phase control of the absorption spectrum," Phys. Rev. A **72**, 013820 (2005).
43. G. S. Agarwal and K. T. Kapale, "Subwavelength atom localization via coherent population trapping," J. Phys. B **39**, 3437–3446 (2006).
44. V. Ivanov and Y. Rozhdestvensky, "Two-dimensional atom localization in a four-level tripod system in laser fields," Phys. Rev. A **81**, 033809 (2010).
45. R. G. Wan and T. Y. Zhang, "Two-dimensional sub-half-wavelength atom localization via controlled spontaneous emission," Opt. Express **19**, 25823–25832 (2011).
46. C. L. Ding, J. H. Li, R. Yu, X. Y. Hao, and Y. Wu, "High-precision atom localization via controllable spontaneous emission in a cycle-configuration atomic system," Opt. Express **20**, 7870–7885 (2012).
47. C. L. Ding, J. H. Li, X. X. Yang, D. Zhang, and H. Xiong, "Proposal for efficient two-dimensional atom localization using probe absorption in a microwave-driven four-level atomic system," Phys. Rev. A **84**, 043840 (2011).
48. P. Meystre and M. Sargent, *Elements of Quantum Optics* (Springer-Verlag, 1999).
49. D. A. Steck, Rubidium 87 D line data, available online at http://steck.us/alkalidata.